minerals

MDPI

Article

Natural Radioactivity and Radiological Hazard Effects from Granite Rocks in the Gabal Qash Amir Area, South Eastern Desert, Egypt

Bahaa M. Emad [1,†], M. I. Sayyed [2], Hamoud H. Somaily [3,4] and Mohamed Y. Hanfi [1,5,*,†]

1 Nuclear Materials Authority, El Maadi, Cairo P.O. Box 530, Egypt; m.nuc2012@yandex.ru
2 Department of Physics, Faculty of Science, Isra University, Amman 11622, Jordan; mabualssayed@ut.edu.sa
3 Research Center for Advanced Materials Science (RCAMS), King Khalid University, P.O. Box 9004, Abha 61413, Saudi Arabia; hhsamily@kku.edu.sa
4 Department of Physics, Faculty of Science, King Khalid University, P.O. Box 9004, Abha 61413, Saudi Arabia
5 Institute of Physics and Technology, Ural Federal University, 620002 Yekaterinburg, Russia
* Correspondence: mokhamed.khanfi@urfu.ru
† These authors contributed equally to this work.

Abstract: The existence of radioactivity linked to the heavy-bearing minerals in building materials—such as granite—has increased attention to the extraction procedure. Granite rocks play an essential economic role in various areas of Egypt. Thus, this study intended to detect the ^{238}U, ^{232}Th, and ^{40}K activity concentrations in the examined granite samples and to determine the corresponding radiological risks associated with the granite. The studied rocks were collected in the Gabal Qash Amir area (south Eastern Desert, Egypt). The obtained results of the activity concentrations for ^{238}U (193 ± 268) Bq/kg, ^{232}Th (63 ± 29) Bq/kg, and ^{40}K (1034 ± 382) Bq/kg indicated that there were moderate concentrations in the investigated samples, which were greater than the worldwide average. The radioactivity levels in the studied granite samples are due to the secondary alteration of radioactive-bearing minerals associated with cracks of granites (secondary minerals in muscovite granites are wolframite, uraninite, uranophane, beta-uranophane, autunite, xenotime, columbite, zircon, and monazite). The radiological risk assessment for the public from the radionuclides that were associated with the studied granite samples was predicted via estimating the radiological hazard factors, such as the radium equivalent content (362 Bq kg^{-1}), compared with the recommended limit. The dosing rate D_{air} in the air (169.2 nGy/h), the annual effective dose both outdoors (AED_{out} ~ 0.21 ± 0.17 mSv) and indoors (AED_{in} ~ 0.83 ± 0.67 mSv), the annual gonadal dose equivalent (AGDE ~ 1.18 ± 0.92 mSv), as well as the external (H_{ex}) and internal (H_{in}) hazard indices (>1), and another factor were associated with excess lifetime cancer risk. According to the statistical investigation, the studied granites were inappropriate for use in construction and infrastructure fields. They may induce health problems due to the radioactivity levels, which exceed the recommended limits.

Keywords: granite rocks; radioactive; terrestrial; radium equivalent content; excess lifetime cancer

Citation: Emad, B.M.; Sayyed, M.I.; Somaily, H.H.; Hanfi, M.Y. Natural Radioactivity and Radiological Hazard Effects from Granite Rocks in the Gabal Qash Amir Area, South Eastern Desert, Egypt. *Minerals* **2022**, *12*, 884. https://doi.org/10.3390/min12070884

Academic Editor: Fernando P. Carvalho

Received: 20 May 2022
Accepted: 7 July 2022
Published: 14 July 2022

1. Introduction

Terrestrial radioactivity and cosmic radiation are the origins of natural radioactivity. The two main types of exposure to humans are external exposure, which is related to gamma rays emitted from terrestrial radionuclides, such as ^{238}U, ^{232}Th, and ^{40}K, and internal exposure from inhaled radon gas and its decay products [1–3].

Numerous analyses have been performed on areas with high natural radioactivity around the world and have come to attention in recent years for risk assessments. The previous studies have illustrated the existence of radionuclides with high concentrations in granite rocks, sediments, and soils, etc. Among various geological items, granite rocks and sediments play a fundamental role in building materials, as well as the accumulation and transportation of radionuclides from one zone to another [4–7].

Anthropogenic impacts, such as U-mining, have led to the elimination of radionuclides, which then disperse into the environment [8–10]. Therefore, the radioactivity levels around mining zones are high compared to other areas and accordingly, the background radiation will increase. Consequently, the long-term exposure to gamma radiation can induce many acute diseases, such as those associated with the kidneys, liver, bones, lungs, and pancreas [11]. Moreover, diseases, such as lung cancer, digestive system cancer, and kidney cancer, can be linked to a variety of pathways, including the inhalation of radon gas and its derivatives, as well as the ingestion of radioactive food [12,13].

Performing a radiological environmental assessment for building components in order to investigate and control the radioactive effects on people and the environment is a large and difficult task that must be caried out in order to fulfill long-term development goals. In order to analyze the radiation consequences, quantifiable factors that may be utilized as input parameters for modeling the environmental dispersion and determining the radiation dosage should be used [14,15].

The investigation area was selected due to the economic value of the heavy radioactive minerals amassed in the granite and sediments rocks, compared to the different areas that have been investigated in Egyptian deserts. The novelty of the current investigation is the detection of the levels of radionuclide concentrations in the investigated granites, which may be involved in infrastructure implementations. In addition, the evaluation of the public exposure to radiation via the assessment of the radiological hazards was detected with different radioactive factors.

2. Geological Description

The Gabal Qash Amir muscovite granite area is found near the Sudan border in Egypt's Eastern Desert, and it makes up the southern part of the Elba topographical sheet (NF-37 I). It is around 27 km southwest of Abu-Ramad city. It is bound by longitudes of 36°14′24″ E–36°10′59″ E and latitudes of 22°15′21″ N–22°14′7″ N. (Figure 1).

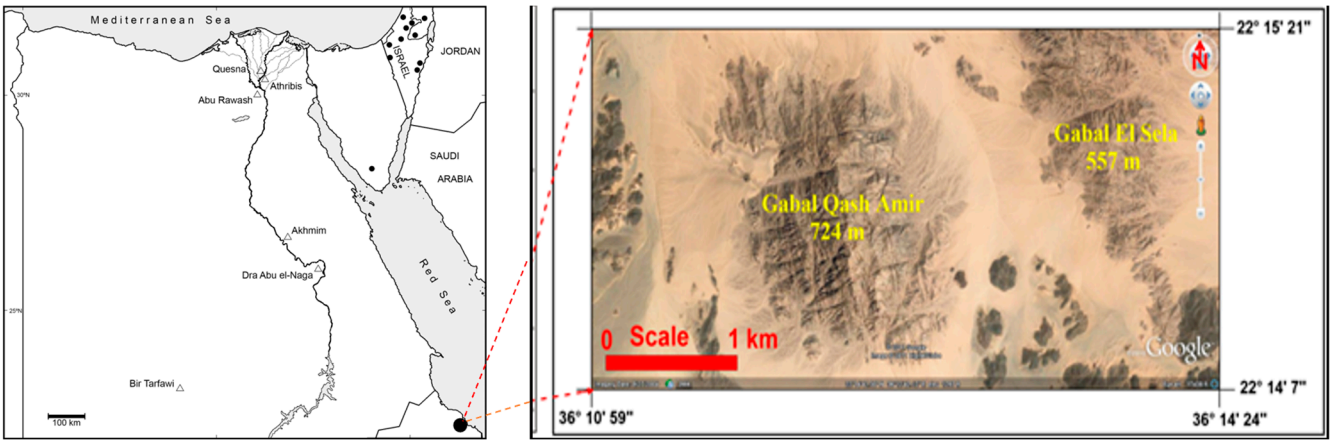

Figure 1. Location map and Google image for the Gabal Qash Amir area.

The study location forms an isolated ovoid pluton with intruding schistose metavolcanic rocks. The pluton outcrops along a NW–SE oriented ridge and it is bordered by wadi sediments (Khalaf, 2005).

Khalaf (2005) concluded that the muscovite granites are a highly-fractionated component of the calc-alkaline granite series, which was deposited in a post-orogenic tectonic setting [16]. The muscovite granite of the studied area, and its environs, were subjected to a thorough geological investigation (Figure 2).

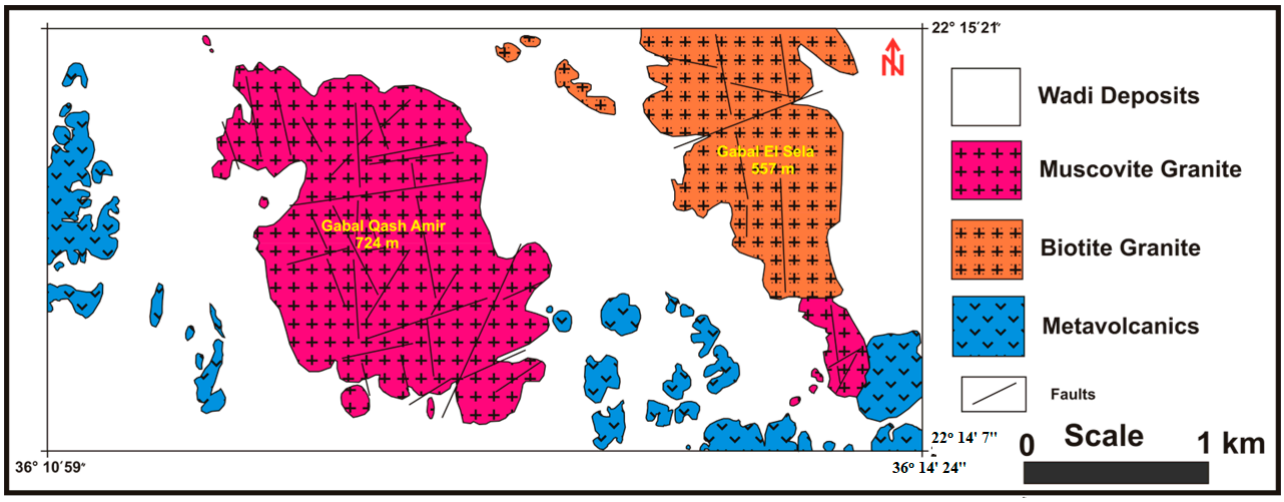

Figure 2. Geological map of the Gabal Qash Amir area, south Eastern Desert, Egypt.

2.1. Metavolcanics

The metavolcanic rocks crop out in the western and southern sectors of the investigated area. The low to moderate relief hills of these rocks are dark-green to greyish-green in color, massive, porphyritic, fine-grained, foliated, extensively jointed, and very schistose in certain parts. They are made up of metavolcanics (dacite, andesite, and rhyolite). The metavolcanics show andesite, dacite, and rhyolite compositions. Meta-agglomerates, banded meta-crystal tuffs, and tuffs are most commonly associated with meta-pyroclastics [17].

According to the field surveys, the biotite and muscovite granites show sharp intrusive contacts with the metavolcanics (Figure 3a).

2.2. Biotite Granite

Low to high granite relief landscapes and isolated scattered granitic blocks are found in this granite. It comes in a variety of colors and grain sizes, ranging from medium to coarse, with a coarse-granite domination. Vertical joints, fractures, and exfoliation are common features (Figure 3b). The primary constituents are biotite, K–feldspar, quartz, plagioclase, and rare muscovite. The fractures of granites include manganese oxides and iron. Radioactive mineralization is produced in the granites, due to hydrothermal alteration. The alteration can be seen as albitization, kaolinization, and hematitization. It intrudes the metavolcanics with intrusive sharp contact, and is invaded by numerous types of dykes e.g., microgranite, bostonite, basic dykes, and veins [18,19].

2.3. Muscovite Granite

The muscovite granite is found in the studied area as moderate to high relief hills (Figure 2). Its color varies from pink to red, and its grain size extends from medium to coarse, with coarse-grained granite dominating. This granite has been heavily worn, exfoliated, and jointed (Figure 3c). N–S, E–W, and NE–SW oriented cracks, joints, and fractures affect this rock. Manganese fracture filling characterizes the pluton's peripheral areas, particularly in the southwestern section.

Various secondary processes (kaolinization, hematization, albitization, and greening tacks) have altered these granites [20,21]. Visible uranophane mineralization can be found along the joint planes. The bostonite dyke cuts through the eastern half of the investigated area of the muscovite granite and is characterized by the crimson to deep-red color; it is heavily jointed and fractured (Figure 3d).

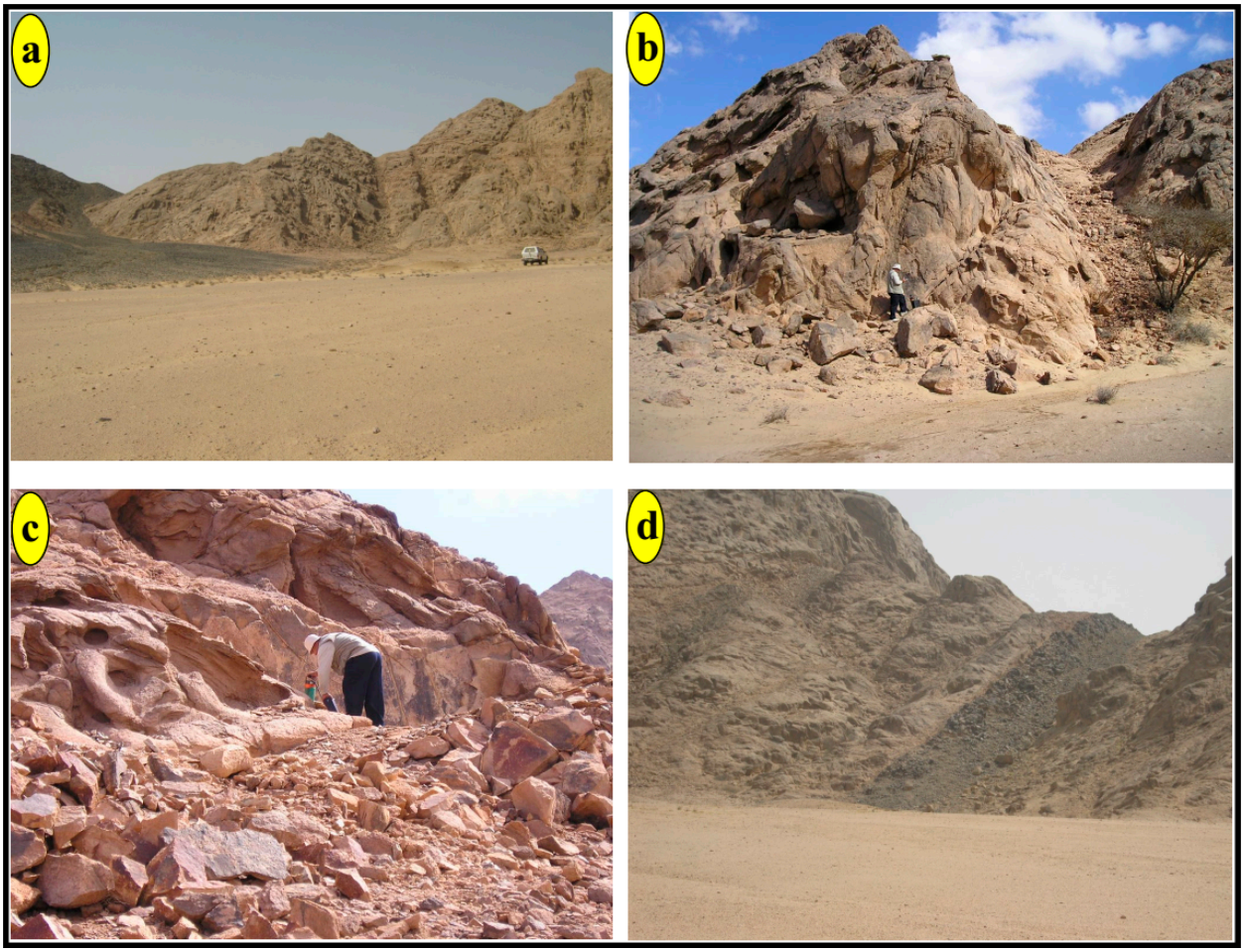

Figure 3. Field photographs of the studied area; (**a**) Sharp intrusive contact among muscovite and metavolcanic granite (SW), (**b**,**c**) Exfoliation, cavernous, and bouldery weathering in biotite and muscovite granite (W, E), and (**d**) Dark-black color basic dyke cut in the western part of the muscovite granite (E).

3. Materials and Methods

3.1. Sampling and Sample Preparation

About 136 chosen samples of muscovite granite were collected regularly from the studied area, utilizing a metallic scoop, and were stored in plastic zip bags. The collected samples were transported into the laboratory, were crushed, and the homogenous samples were sieved below 200 meshes. The samples were stored in plastic containers with a known volume of 250 cm^3 for twenty-eight days, after which the radon gas and its daughters had reached secular radioactive equilibrium.

3.2. Gamma-Ray Spectroscopic Analysis

The radioactivity in the storage samples was detected via a solid-state detector, namely, a hyper pure germanium (HPGe) detector. The analysis of the samples was conducted regularly, in which each sample was measured for approximately 20 h. The detection of radioactivity in the examined samples relied on the resolution of the HPGe detector. The resolution was detected at 1.85 and 1332.5 for ^{226}Ra and ^{60}Co, respectively. Before the measurement of radioactivity in the granite samples was taken, calibration of the HPGe detector was conducted utilizing various radioactive approved sources, such as ^{226}Ra, ^{60}Co, and ^{241}Am (USA, 1994, approved the standard sources), and the efficiency curve was presented with two phases, with an energy range of 186–2450 keV. The ^{226}Ra point source was applied to determine the relative efficiency curve. At the same time, in the other phase,

the normalization of the relative curve of the spectrometer was achieved with potassium chloride. After the calibration, and before the measurements were taken, the background radiation was detected via a blank vessel with an identical volume and was estimated at an identical duration. Finally, after the detection, the activity of the radionuclide was determined by the following Formula (1) [22]:

$$A = \frac{N/t}{\varepsilon I_\gamma m} \quad (1)$$

where A refers to the activity of the radionuclide (Bq kg^{-1}), N denotes the full-energy peak's total net count (by subtracting the background area from the overall area, the peak areas are found), t shows the duration of the count (Sec), ε represents the efficiency of the HPGe detector, I_γ refers to the γ-abundance, and m is the mass of the measured sample (kg). The detection of ^{238}U in the granite samples was analyzed by determining ^{226}Ra (186 keV), ^{214}Pb (0.352, 0.295 MeV), ^{234}Pa (1.001 MeV), and ^{214}Bi (0.609, 1.120, 1.765 MeV), while the ^{232}Th activity concentration was determined from its decay products at energies of 0.911, 0.338 MeV for ^{228}Ac and 0.583, 2.614 MeV for Tl. Furthermore, the ^{40}K activity concentrations were detected at photopeak energy (1.460 MeV) [23]. To eliminate any inaccuracy in the ray intensities, and the influence of coincidence summation, the efficiency calibration of the spectrometry system was performed utilizing the radionuclide-specific efficiency approach. Certified reference materials, such as RGU-1, RGTh-1, and RGK-1, were employed; their densities were equal to that of the building materials after pulverization [24]. The container geometry was selected according to the sample type in order to distribute the samples homogeneously. The ^{226}Ra, ^{232}Th, and ^{40}K had MDAs of 2, 4, and 12 Bq kg^{-1}, respectively. Total radiation level uncertainty was estimated using systematic and random detection errors. Random errors of up to 5% were found in radioactivity readings, and regular mistakes of 0.5 to 2% were found in efficiency calibration [25]. After the detection of activity concentrations of ^{238}U, ^{232}Th, and ^{40}K, the radiological variables were estimated according to Table 1.

Table 1. Important radiological parameters and indices [26,27].

Parameter	Definition	Formula
Ra_{eq}	The radium equivalent content (Ra_{eq}) is a radioactive parameter that is widely applied in radiation health hazards. The results of Ra_{eq} must be less than 370 Bq kg^{-1}, which keeps the AED for the public lower than one mSv.	Ra_{eq} (Bq kg^{-1})= A_{Ra} + 1.43 A_{Th} + 0.077 A_K
D (nGy/h)	The radioactive factor known as the absorbed dose rate is used to evaluate the effect of gamma radiation at a distance of 1 m from radiation sources in the air, owing to the concentrations of ^{238}U, ^{232}Th, and ^{40}K.	D_{air} (nGy h^{-1}) = 0.430 A_U + 0.666 A_{Th} + 0.042 A_K
AEDout	An element of radioactivity called the yearly effective dose is used to gauge radiation exposure levels over a fixed period of time (1 year).	AED_{out} (mSv/y) = D_{air} (nGy/h) × 0.2 × 8760 (h/y) × 0.7 (Sv/Gy) × 10^{-6} (mSv/nGy)
AEDin		AED_{in} (mSv/y) = D_{air} (nGy/h) × 0.8 × 8760 (h/y) × 0.7 (Sv/Gy) × 10^{-6} (mSv/nGy)
H_{ex}	The radiological parameters used to evaluate the risk of gamma radiation are known as the external hazard index. When radon and its decay products are exposed internally, the internal hazard index is used.	$H_{ex} = \frac{A_U}{370} + \frac{A_{Th}}{259} + \frac{A_K}{4810}$
H_{in}		$H_{in} = \frac{A_U}{185} + \frac{A_{Th}}{259} + \frac{A_K}{4810}$
Iγ	Due to the various combinations of distinct natural activities in the sample, another index was proposed by a group of specialists to determine the amount of radiation hazard linked with the natural radionuclides in the samples.	$I_\gamma = \frac{A_{Ra}}{150} + \frac{A_{Th}}{100} + \frac{A_K}{1500}$
AGDE	The radioactive measure known as the yearly gonadal dose equivalent is used to calculate the doses of gamma radiation that are absorbed by the gonads.	AGDE (mSv y^{-1}) = 3.09A_{Ra} + 4.18A_{Th} + 0.314A_K
ELCR	The radioactive factor used to determine whether gamma radiation exposure has caused lethal cancer is called excess lifetime cancer.	ELCR = AED_{out} × DL × RF

4. Results and Discussion

4.1. Radioactivity in Granites

Table S1 displays the ^{238}U, ^{232}Th, and ^{40}K activity concentrations that were detected in the granite samples. Table 2 depicts the activity concentration means of the ^{238}U, ^{232}Th, and ^{40}K samples have surpassed the worldwide averages of 35, 45, and 412, respectively [3]. As elucidated in the investigated granite samples, the mean of A_U was 193 ± 268 Bq kg$^{-1,}$ greater than the mean reported value (33 Bq kg^{-1}), with a factor of approximately six. It ranged from 22 to 2099 Bq kg^{-1}, while the mean of A_{Th} was 63 ± 29 Bq kg^{-1}, which is higher by a factor of 1.4 compared to the 45 Bq kg^{-1} worldwide average, and its minimum value was 10 Bq kg^{-1}. The maximum value was 183 Bq kg^{-1}. The values of the A_K were altered from 125 to 1659 Bq kg^{-1}, with a mean value of 1034 ± 382 Bq kg^{-1}, which is greater by a factor of 2.5 compared to the worldwide average (412 Bq kg^{-1}). The skewness values of ^{238}U and ^{232}Th activity concentrations were positive and demonstrate a positive asymmetric nature. In contrast, a negative asymmetric distribution was displayed in the skewness values of the ^{40}K activity concentration. Additionally, the kurtosis values reflect the distribution probability's peak. Table 1 illustrates that the kurtosis values are positive for the ^{238}U and ^{232}Th activity concentrations (the distributions are peaked). The activity concentration distribution of ^{40}K is flat, due to the fact that the kurtosis values are negative.

Table 2. Basic statistical summary of muscovite granite rocks, Gabal Qash Amir, Egypt.

Variables *	U-238	Th-232	K-40	Ra_{eq}	H_{in}	H_{ex}	Iγ	D_{air}	AED_{out}	AED_{in}	AGDE	ELCR
	(Bq/kg)	(Bq/kg)	(Bq/kg)	(Bq/kg)				nGy/h	mSv	mSv	mSv	
N	136	136	136	136	136	136	136	136	136	136	136	136
Mean	193	63	1034	362	1.50	0.98	1.30	169.2	0.21	0.83	1.18	0.0007
SD	268	29	382	298.21	1.52	0.81	1.01	137.0	0.17	0.67	0.92	0.0006
Min	22.23	9.74	125.20	65.09	0.24	0.18	0.25	31.56	0.04	0.15	0.23	0.0001
Max	2099.50	182.70	1658.90	2351.01	12.03	6.35	7.89	1078	1.32	5.29	7.24	0.0046
Skew	4.19	0.77	−0.46	3.41	3.82	3.41	3.25	3.37	3.37	3.37	3.27	3.37
Kurtosis	22.15	2.69	−1.04	16.79	19.57	16.80	15.68	16.45	16.45	16.45	15.81	16.45

* N = Number; SD = Standard deviation; Max = Maximum; Min = Minimum; Skew = Skewness.

The frequency distribution of A_U, A_{Th}, and A_K are presented in Figure 4. However, the ^{238}U, ^{232}Th, and ^{40}K activity concentrations displayed a multi-modality degree. This illustrates that the granites were enriched with various radioactive-bearing minerals; thus, this study needs to analyze the minerals. The present results of A_U, A_{Th}, and A_K are compared with other studies in various countries (Table 3).

Figure 5 exhibits a map for the granite samples with the A_U, A_{Th}, and A_K. The proportion A_U/A_{Th} indicates that the granite has been enriched with uranium as a result of rainwater leaching, which has aided in the movement of uranium minerals and precipitation at faults and joints [10].

As shown in Figure 5, the highest uranium activity concentrations were found in the examined samples that were collected from the southeastern region of the studied area. This is linked to the disruption of radioactive materials that have been deposited inside of the granite fissures. Moreover, several of the analyzed areas had high thorium activity concentrations. This is due to the presence of several minerals in the granite samples, such as thorianite, zircon, and monazite.

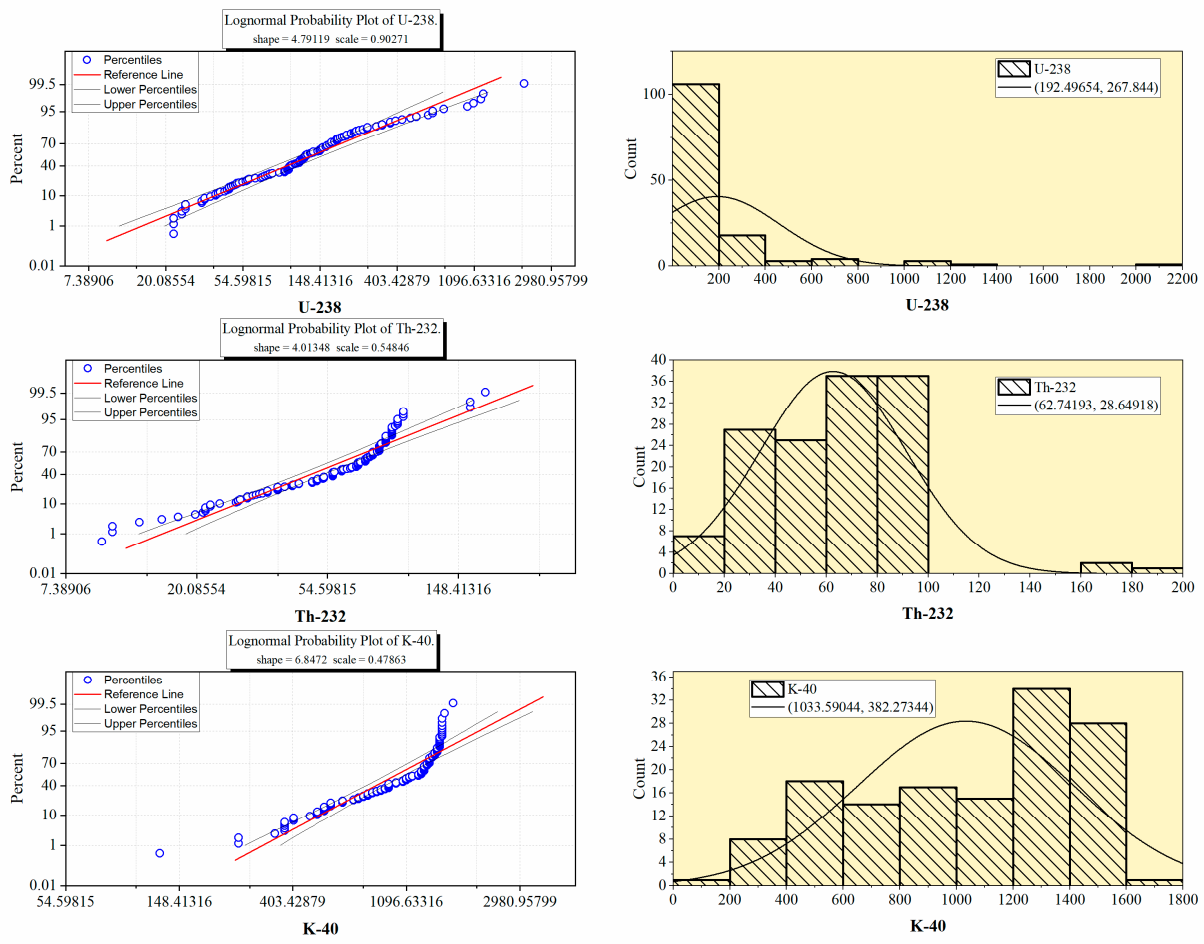

Figure 4. The distribution of ^{238}U, ^{232}Th, and ^{40}K activity concentrations of the muscovite granite rocks in the studied area.

Table 3. Comparison of ^{238}U, ^{232}Th, and ^{40}K activity concentrations in the Gabal Qash Amir area with other studies of different countries.

Country	^{238}U	^{232}Th	^{40}K	References
Egypt	193	63	1034	Present study
Egypt	137	82	1082	[28]
Saudi Arabia	28.82	34.83	665.08	[29]
Palestine	71	82	780	[30]
Jordan	41.52	58.42	897	[31]
India	25.88	42.82	560.6	[32]
Iran	77.4	44.5	1017.2	[33]
Spain	84	42	1138	[34]
Greece	74	85	881	[25]
Turkey	80	101	974	[35]
Nigeria	63.29	226.67	832.59	[1]
Italy	85.86	24.71	1340.49	[36]

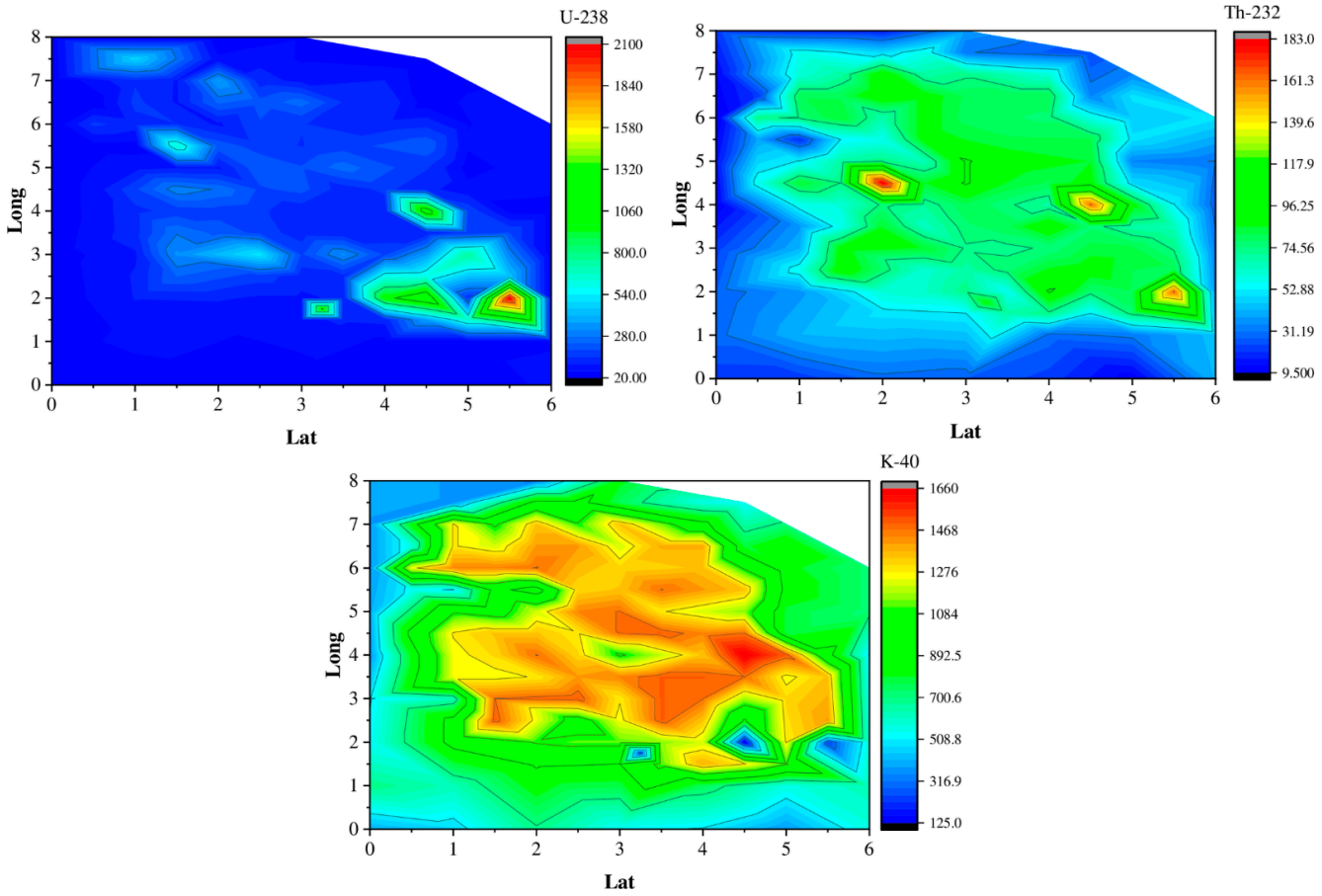

Figure 5. The distribution map of the accumulation of high concentrations of ^{238}U, ^{232}Th, and ^{40}K of the muscovite granites in the investigated area.

4.2. Radioactive Assessment

The Ra_{eq} values in the granite samples are computed and presented in Figure 6. As reported in Figure 6, 34% of the examined samples represent higher values of Ra_{eq} than 370 Bq kg^{-1}. The Ra_{eq} mean value was 362 Bq kg^{-1}, which is comparable with the recommended limit, and the Ra_{eq} values ranged from 65.09 to 2351.01 Bq kg^{-1} in the examined granite. The highest Ra_{eq} reveals the presence of U and Th in the examined granite with high activity concentrations.

The results of D_{air} reveal that the highest D_{air} values were detected in the granite samples from the southeastern region of the studied area. Statistically, the D_{air} data changed from 31.56 to 1078 nGy/h, with the mean value being 169.2 ± 137.0 nGy/h above the approved limit (59 nGy/h) [3,37]. This displays that the granites of the Gabal Qash Amir area are inappropriate for various infrastructure fields. This leads to evaluating the public exposure from the investigated granites. Based on the D_{air} data of the examined granites, the AED values were estimated based on two scenarios and are displayed in Table S1. Table 2 illustrates that the AED_{out} values varied from 0.04 to 1.32 mSv, with a mean value of 0.21 ± 0.17 mSv, > 0.07 mSv (recommended limit) [3], while 0.15 and 0.67 mSv are the Min and Max values of the AED_{in}, respectively, with a mean value of 0.83 ± 0.67 mSv, which is two times that of the recommended value of 0.41 mSv. Moreover, long-term exposure to huge dosages might cause tissue degeneration, cancer, coronary heart disease, and may impact deoxyribonucleic acid (DNA) in genes [38].

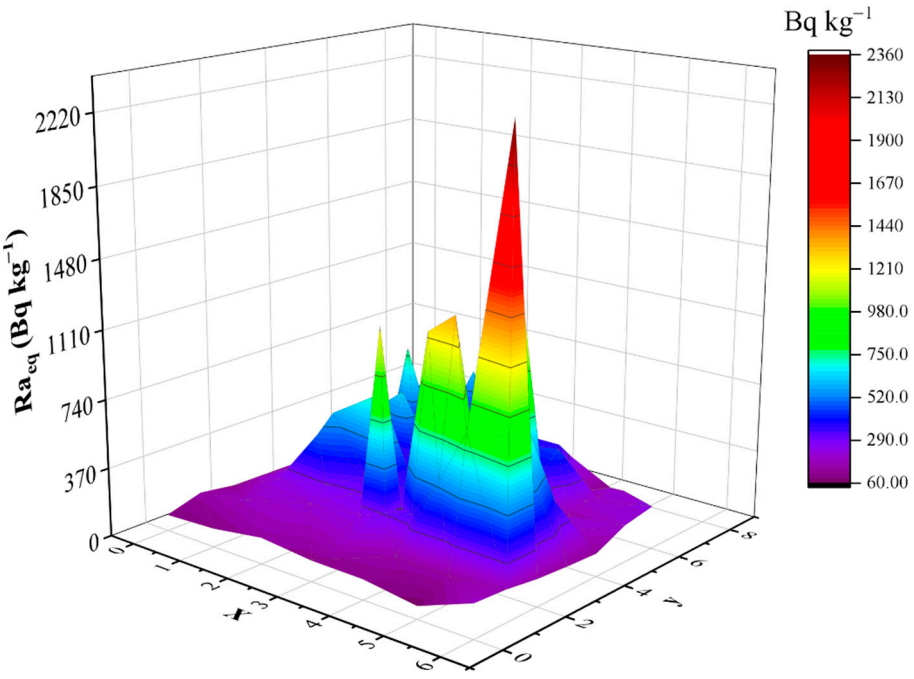

Figure 6. The radium equivalent content (Ra_{eq}) of the investigated muscovite granites in the studied area.

The significant health risks can be detected with higher radiological hazard indices. In the current study, H_{ex} data ranged from 0.18 to 6.35, with a mean value of 0.98, which is comparable to the recommended value ($H_{ex} \leq 1$), while the maximum value of H_{in} in the investigated granites was 12.03 and the minimum was 0.24, with a mean value 1.5, which is higher than the recommended value ($H_{in} \leq 1$). Consequently, a significant risk can be observed due to the internal hazard index. This indicates that health effects, stemming from the inhalation of emitted radon gas and its decay products from the granite rocks, will be observed [39].

The range of I_γ values in the investigated granite samples varied between 0.25 and 7.89 for the minimum and maximum values, respectively. The high I_γ values show that the granite samples in the southeastern half of the study area provide a considerable health risk and, thus, are not compatible for use in construction materials.

The AGDE data were calculated for all of the granite samples and are shown in Table S1 and the consistent descriptive statistics are shown in Table 1. The range of AGDE values altered between 0.23 (Sample number S9 and S14) and 7.24 (Sample number 126) mSv y^{-1}. The mean value was 1.18 ± 0.92 mSv y^{-1}, which is four times higher than the limit of 0.3 mSv y^{-1} [3]. Thus, the granite rocks in the investigated area are inconvenient for masonry materials.

Moreover, the ELCR values of the granite rocks studied here show a range of 0.0001 to 0.0046, with a mean value of 0.0007, which is two times greater than the maximum limit (0.00029) [40]. This demonstrates that public exposure to the investigated granite causes cancer effects over the course of their lives.

4.3. Statistical Analysis

The study divides the association between natural radioactive indicators into two components. First, the correlation between A_U, A_{Th}, and A_K with the Ra_{eq} was studied and is plotted in Figure 7a–c. A strong positive correlation (R^2 = 0.96) between the Ra_{eq} and ^{238}U activity concentrations was found. A good correlation (R^2 = 0.53) between Ra_{eq} and ^{232}Th activity concentrations was also found, while there was a weak correlation (R^2 = 0.04) with ^{40}K. The correlation of Ra_{eq} with the natural radionuclide activity concentrations

indicates that the granite rock is enriched with uranium, which is the main contribution to Ra_{eq}. This establishes the geological properties of the granite rocks in the investigated zone, where weathering has caused the occurrence of heavy radioactive minerals, including thorite, uranophane autunite, and uranothorite.

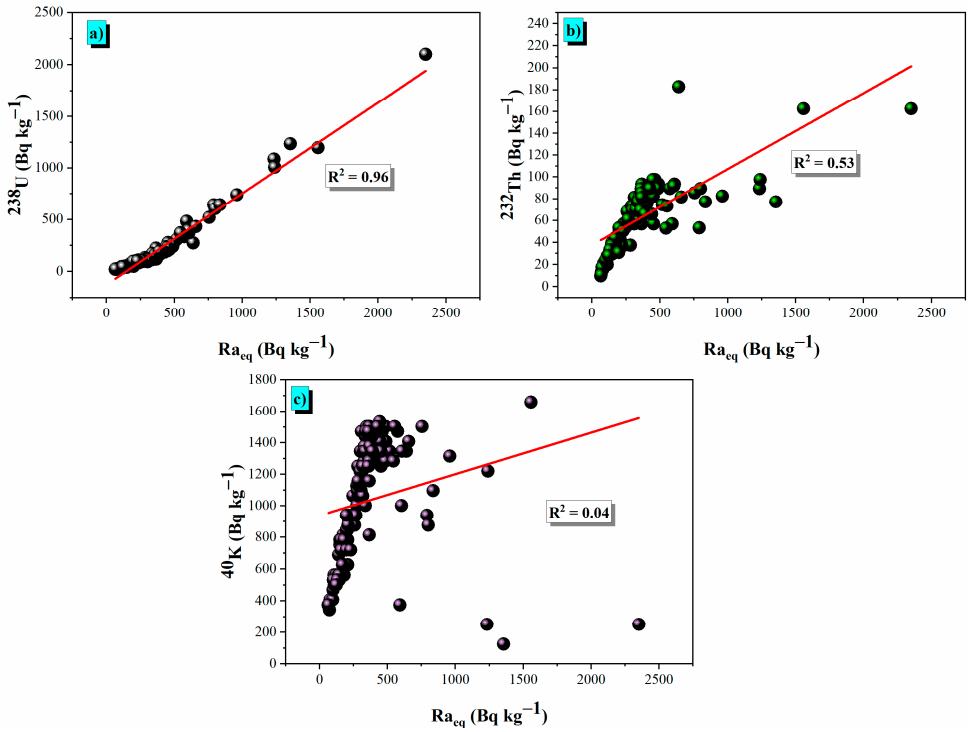

Figure 7. The correlation between the radium equivalent content and the activity concentrations of (**a**) ^{238}U, (**b**) ^{232}Th, and (**c**) ^{40}K in the muscovite granites.

Moreover, rare metals are contained in monazite, zircon, samarskite, xenotime, columbite, rutile, fergusonite, and fluorite [16]. Second, the Pearson correlation was used to look at the links between the natural radioactivity and the radiological risks (Table 4). The Pearson correlation shows a substantial link among all of the radiological hazard indices and ^{238}U, and a strong correlation with ^{232}Th, because the ^{238}U and ^{232}Th series are naturally associated together. Furthermore, a weak correlation was found between the radiological parameters and the ^{40}K activity concentration. This emphasizes that the granitic rocks with significant uranium activity are accountable for the radioactive hazards and health risks.

Table 4. Pearson correlation between natural radionuclides and the radiological hazard coefficients of muscovite granite rocks, Gabal Qash Amir, Egypt.

	U-238	Th-232	K-40	Ra_{eq}	H_{in}	H_{ex}	Iγ	D_{air}	AED_{out}	AED_{in}	ELCR	AGDE
U-238	1											
Th-232	0.58	1										
K-40	0.02	0.67	1									
Ra_{eq}	0.98	0.73	0.21	1								
H_{in}	0.99	0.66	0.12	0.99	1							
H_{ex}	0.98	0.73	0.20	0.99	1.00	1						
Iγ	0.97	0.74	0.24	0.99	0.99	0.99	1					
D_{air}	0.98	0.73	0.21	0.99	0.99	0.99	0.99	1				
AED_{out}	0.98	0.73	0.21	0.99	0.99	0.99	0.99	1	1			
AED_{in}	0.98	0.73	0.21	0.99	0.99	0.99	0.99	1	1	1		
ELCR	0.98	0.73	0.21	0.99	0.99	0.99	0.99	1	1	1	1	
AGDE	0.97	0.74	0.23	0.99	0.99	0.99	0.99	0.99	0.99	0.99	0.99	1

The PCA (principal component analysis) used varimax rotations in order to control the correlation matrix between several items. In Figure 8, the PC1 and PC2 components are provided and plotted. The A_U is highly positive in the PC1 loading, correlating with all of the radioactive variables, and is explained with a variance of 87.83%. This indicates that the A_U is the primary source of the natural radioactivity in the granitic rocks studied here.

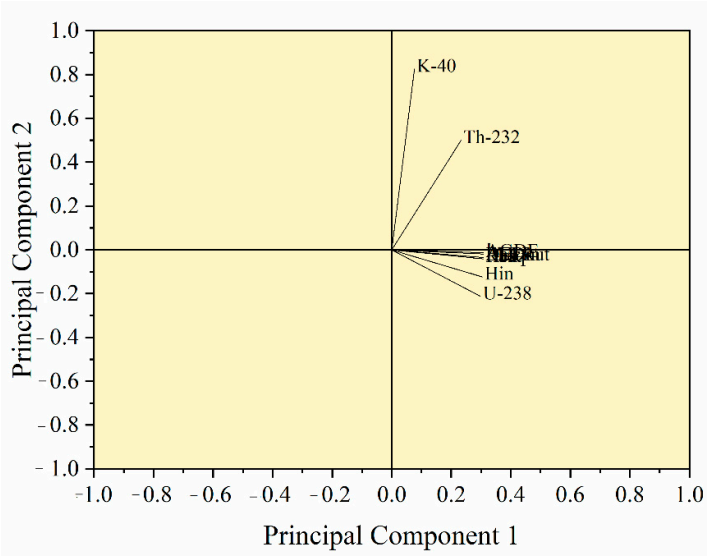

Figure 8. Principal component analysis (PC1 and PC2) for the radiological data.(the overlapping parts are Ra_{eq}, H_{ex}, Iγ, D_{air}, AED_{out}, AED_{in}, ELCR and AGDE from top to bottom).

The PC2 load, on the other hand, is weakly positive for A_{Th} and strongly negative for A_K, which is explained with a variance of 10.98%. As can be seen, the loading variance is positive, which is explained by the fact that ^{232}Th and ^{40}K do not affect the radiation exposure grade. The total explained variance in the PC analysis is 98.81%, indicating that the radioactive data proved to be good [41].

The correlations between the radiological parameters have been studied by applying hierarchical clustering analysis (HCA) and are plotted in Figure 9.

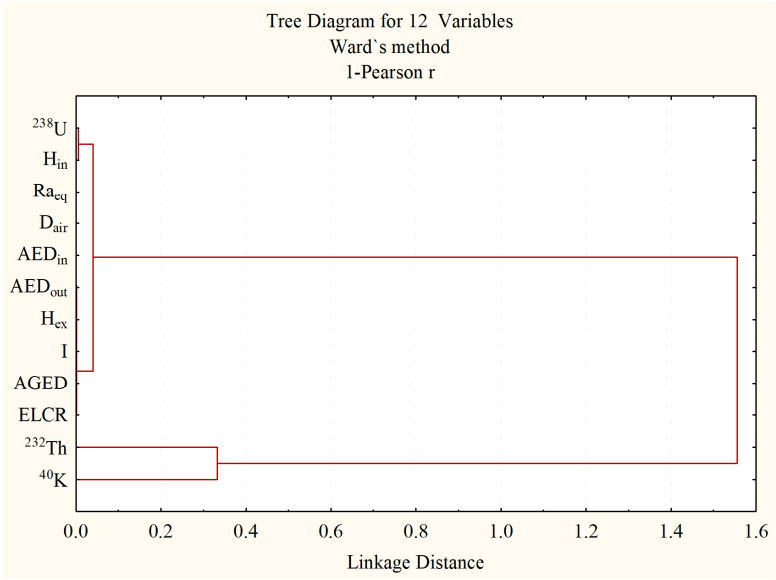

Figure 9. The hierarchical clustering analysis (HCA) of the radiological parameters.

The dendrogram of the results is divided into two clusters. Cluster I contains ^{232}Th and ^{40}K, whereas cluster II comprises the rest of the radiological variables. The application

of HCA indicates that the radioactivity of the granitic rocks is attributed to the activity concentration of ^{238}U. The HCA agrees with the other statistical investigations, such as the Pearson analysis and the PCA.

5. Conclusions

The goal of this study was to produce a comprehensive assessment of the radioactivity associated with granite rocks that can be applied in building materials and infrastructure fields. A statistical study was carried out in order to show the geological processes that result in a rise in radioactive content in granite rocks. The activity concentrations of 193, 63, and 1034 Bq kg^{-1} of A_U, A_{Th}, and $A_{K,}$ respectively, are moderate concentrations and are greater than the mean worldwide value. Moreover, all of the radiological hazard parameters were detected in the studied samples and displayed greater values than the recommended levels. This is attributed to the existence of radioactive-bearing minerals and rare metals in the investigated granite rocks. The granite in the examined area is not appropriate to consume and should not be employed in construction materials or in infrastructure applications.

Supplementary Materials: The following supporting information can be downloaded at: https://www.mdpi.com/article/10.3390/min12070884/s1, Table S1: The concentrations of radionuclides ^{238}U, ^{232}Th, ^{40}K and the radiological hazard indices.

Author Contributions: Conceptualization, B.M.E. and M.Y.H.; methodology, B.M.E. and M.Y.H.; software, M.I.S. and M.Y.H.; validation, H.H.S.; formal analysis, M.Y.H.; investigation, M.I.S.; resources, B.M.E. and M.Y.H.; data curation, B.M.E. and M.Y.H.; writing—original draft preparation, B.M.E. and M.Y.H.; writing—review and editing, B.M.E. and M.Y.H.; visualization, B.M.E., M.I.S., and M.Y.H.; supervision, M.I.S.; project administration, B.M.E. and M.Y.H.; funding acquisition, H.H.S. All authors have read and agreed to the published version of the manuscript.

Funding: This work was supported by King Khalid University through a grant (KKU/RCAMS/22) under the Research Center for Advanced Materials Science (RCAMS) at King Khalid University, Saudi Arabia.

Institutional Review Board Statement: Not applicable.

Informed Consent Statement: Not applicable.

Data Availability Statement: Not applicable.

Acknowledgments: The authors would like to thank the Nuclear Materials Authority, Egypt. This work was supported by King Khalid University through a grant (KKU/RCAMS/22) under the Research Center for Advanced Materials Science (RCAMS) at King Khalid University, Saudi Arabia.

Conflicts of Interest: The authors declare no conflict of interest.

References

1. Akpanowo, M.A.; Umaru, I.; Iyakwari, S.; Joshua, E.O.; Yusuf, S.; Ekong, G.B. Determination of natural radioactivity levels and radiological hazards in environmental samples from artisanal mining sites of Anka, North-West Nigeria. *Sci. Afr.* **2020**, *10*, e00561. [CrossRef]
2. Hanfi, M.Y.; Yarmoshenko, I.; Seleznev, A.A.; Onishchenko, A.D.; Zhukovsky, M.V. Development of an appropriate method for measuring gross alpha activity concentration in low-mass size-fractionated samples of sediment using solid-state nuclear track detectors. *J. Radioanal. Nucl. Chem.* **2020**, *323*, 1047–1053. [CrossRef]
3. UNSCEAR. *Sources and Effects of Ionizing Radiation—Exposures of the Public and Workers from Various Sources of Radiation*; UNSCEAR 2008 Report; UNSCEAR: New York, NY, USA, 2010.
4. Gaafar, I.; Hanfi, M.; El-Ahll, L.S.; Zeidan, I. Assessment of radiation hazards from phosphate rocks, Sibaiya area, central eastern desert, Egypt. *Appl. Radiat. Isot.* **2021**, *173*, 109734. [CrossRef] [PubMed]
5. Sivakumar, S.; Chandrasekaran, A.; Senthilkumar, G.; Suresh Gandhi, M.; Ravisankar, R. Determination of radioactivity levels and associated hazards of coastal sediment from south east coast of Tamil Nadu with statistical approach. *Iran. J. Sci. Technol. Trans. A Sci.* **2018**, *42*, 601–614. [CrossRef]
6. Awad, M.; El Mezayen, A.M.; El Azab, A.; Alfi, S.M.; Ali, H.H.; Hanfi, M.Y. Radioactive risk assessment of beach sand along the coastline of Mediterranean Sea at El-Arish area, North Sinai, Egypt. *Mar. Pollut. Bull.* **2022**, *177*, 113494. [CrossRef]

7. Khandaker, U.M.; Asaduzzaman, K.; Bin Sulaiman, A.F.; Bradley, D.A.; Isinkaya, M.O. Elevated concentrations of naturally occurring radionuclides in heavy mineral-rich beach sands of Langkawi Island, Malaysia. *Mar. Pollut. Bull.* **2018**, *127*, 654–663. [CrossRef]
8. Hanfi, M.Y.; Yarmoshenko, V.; Seleznev, A.A.; Malinovsky, G.; Ilgasheva, E.; Zhukovsky, M.V. Beta radioactivity of urban surface–deposited sediment in three Russian cities. *Environ. Sci. Pollut. Res.* **2020**, *27*, 40309–40315. [CrossRef]
9. El-Kammar, A.M.; Salman, A.E.; Shalaby, M.H.; Mahdy, A.I. Geochemical and genetical constraints on rare metals mineralization at the central Eastern Desert of Egypt. *Geochem. J.* **2001**, *35*, 117–135. [CrossRef]
10. Nagar, M.S.; Bayoumi, B.M.; Morsy, W.M. Characteristics and Evaluation of Leaching Behavior of Uranium Mineralization in Qash Amir Granite, South Eastern Desert. *Egypt. Am. J. Appl. Ind. Chem.* **2021**, *5*, 7–16. [CrossRef]
11. ATSDR. *Case Studies in Environmental Medicine*; Public Health Service of U.S. Department of Health and Human Services: Washington, DC, USA, 1992; pp. 1–28.
12. ATSDR. *Toxicological Profile for Uranium*; Public Health Service of U.S. Department of Health and Human Services: Washington, DC, USA, 1999; pp. 1–145.
13. ATSDR. *Draft Toxicological Profile for Radon: Agency for Toxic Substances and Disease Registry*; ATSDR: Atlanta, GA, USA, 2012; pp. 9–11, 161–167.
14. La Verde, G.; Raulo, A.; D'Avino, V.; Roca, V.; Pugliese, M. Radioactivity content in natural stones used as building materials in Puglia region analysed by high resolution gamma-ray spectroscopy: Preliminary results. *Constr. Build. Mater.* **2020**, *239*, 117668. [CrossRef]
15. Sahoo, B.K.; Nathwani, D.; Eappen, K.P.; Ramachandran, T.V.; Gaware, J.J.; Mayya, Y.S. Estimation of radon emanation factor in Indian building materials. *Radiat. Meas.* **2007**, *42*, 1422–1425. [CrossRef]
16. Khalaf, I.M. Geology of the area around G. Qash Amir with special emphases on the granitic rocks, south Eastern Desert, Egypt. *Egypt J. Geol.* **2005**, *49*, 49–64.
17. El Mezayen, A.M.; Heikal, M.A.; El-Feky, M.G.; Shahin, H.A.; Abu Zeid, I.K.; Lasheen, S.R. Petrology, geochemistry, radioactivity, and M–W type rare earth element tetrads of El Sela altered granites, south eastern desert, Egypt. *Acta Geochim.* **2019**, *38*, 95–119. [CrossRef]
18. Gaafar, I.M.; Aboelkhair, H.M.; Bayoumi, M.B. Integration of Gamma-Ray Spectrometric and Aster Data for Uranium Exploration in Qash Amer-EL-Sela Area, Southeastern Desert, Egypt. *Nucl. Sci. Sci. J.* **2017**, *6*, 17–33. [CrossRef]
19. Nagar, M.S.; Shahin, H.A.; Bahige, M. Column Percolation Leaching of Uranium from El-Sela Area, South Eastern Desert, Egypt. *Res. Rev. J. Chem.* **2016**, *5*, 32–41.
20. Ramadan, T.M.; Ibrahim, T.M.; Said, A.D.; Baiumi, M. Application of remote sensing in exploration for uranium mineralization in Gabal El Sela area, South Eastern Desert, Egypt. *Egypt. J. Remote Sens. Space Sci.* **2013**, *16*, 199–210. [CrossRef]
21. El Arabi, A.M.; Ahmed, N.K.; Din, K.S. Assessment of terrestrial gamma radiation doses for some Egyptian granite samples. *Radiat. Prot. Dosim.* **2008**, *128*, 382–385. [CrossRef]
22. Al-Zahrani, J.H. Journal of Radiation Research and Applied Sciences Estimation of natural radioactivity in local and imported polished granite used as building materials in Saudi Arabia. *J. Radiat. Res. Appl. Sci.* **2017**, *10*, 241–245. [CrossRef]
23. Merdano, B. Radioactivity concentrations and dose assessment for soil samples from kestanbol granite area. *Radiat. Prot. Dosim.* **2006**, *121*, 399–405. [CrossRef]
24. IAEA. *Preparation and Certification of IAEA Gamma-Ray Spectrometry Reference Materials RGU-1, RGTh-1 and RGK-1*; IAEA: Vienna, Austria, 1987; Volume 148, p. 48.
25. Papadopoulos, A.; Christofides, G.; Koroneos, A.; Papadopoulou, L.; Papastefanou, C.; Stoulos, S. Natural radioactivity and radiation index of the major plutonic bodies in Greece. *J. Environ. Radioact.* **2013**, *124*, 227–238. [CrossRef]
26. El Dabe, M.M.; Ismail, A.M.; Metwaly, M.; Taalab, S.A.; Hanfi, M.Y.; Ene, A. Hazards of Radioactive Mineralization Associated with Pegmatites Used as Decorative and Building Material. *Materials* **2022**, *15*, 1224. [CrossRef] [PubMed]
27. Adel, E.A.H.; El-Feky, M.G.; Taha, S.H.; El Minyawi, S.M.; Sallam, H.A.; Ebyan, O.A.; Yousef, E.S.; Hanfi, M.M. Natural Radionuclide Concentrations by γ-Ray Spectrometry in Granitic Rocks of the Sol Hamed Area, Southeastern Desert of Egypt, and Their Radiological Implications. *Minerals* **2022**, *12*, 294. [CrossRef]
28. Amin, R.M. Gamma radiation measurements of naturally occurring radioactive samples from commercial Egyptian granites. *Environ. Earth Sci.* **2012**, *67*, 771–775. [CrossRef]
29. AlZahrani, J.H.; Alharbi, W.R.; Abbady, A.G.E. Radiological impacts of natural radioactivity and heat generation by radioactive decay of phosphorite deposits from Northwestern Saudi Arabia. *Aust. J. Basic Appl.* **2011**, *5*, 683–690.
30. Thabayneh, K.M. Measurement of natural radioactivity and radon exhalation rate in granite samples used in palestinian buildings. *Arab. J. Sci. Eng.* **2013**, *38*, 201–207. [CrossRef]
31. Sharaf, J.M.; Hamideen, M.S. Measurement of natural radioactivity in Jordanian building materials and their contribution to the public indoor gamma dose rate. *Appl. Radiat. Isot.* **2013**, *80*, 61–66. [CrossRef]
32. Senthilkumar, G.; Raghu, Y.; Sivakumar, S.; Chandrasekaran, A.; Prem Anand, D.; Ravisankar, R. Natural radioactivity measurement and evaluation of radiological hazards in some commercial flooring materials used in Thiruvannamalai, Tamilnadu, India. *J. Radiat. Res. Appl. Sci.* **2014**, *7*, 116–122. [CrossRef]
33. Abbasi, A. Calculation of gamma radiation dose rate and radon concentration due to granites used as building materials in Iran. *Radiat. Prot. Dosimetry* **2013**, *155*, 335–342. [CrossRef]

34. Guillén, J.; Tejado, J.J.; Baeza, A.; Corbacho, J.A.; Muñoz, J.G. Assessment of radiological hazard of commercial granites from Extremadura (Spain). *J. Environ. Radioact.* **2014**, *132*, 81–88. [CrossRef]
35. Aykamiş, A.Ş.; Turhan, S.; Aysun Ugur, F.; Baykan, U.N.; Kiliç, A.M. Natural radioactivity, radon exhalation rates and indoor radon concentration of some granite samples usedas construction material in Turkey. *Radiat. Prot. Dosim.* **2013**, *157*, 105–111. [CrossRef]
36. Caridi, F.; D'Agostino, M.; Marguccio, S.; Belvedere, A.; Belmusto, G.; Marcianò, G.; Sabatino, G.; Mottese, A. Radioactivity, granulometric and elemental analysis of river sediments samples from the coast of Calabria, south of Italy. *Eur. Phys. J. Plus* **2016**, *131*, 136. [CrossRef]
37. USEPA. *EPA Radiogenic Cancer Risk Models and Projections for the U.S. Population*; USEPA: Washington, DC, USA, 2011.
38. Yasmin, S.; Barua, B.S.; Khandaker, M.U.; Kamal, M.; Rashid, A.; Sani, S.F.A.; Ahmed, H.; Nikouravan, B.; Bradley, D.A. The presence of radioactive materials in soil, sand and sediment samples of potenga sea beach area, Chittagong, Bangladesh: Geological characteristics and environmental implication. *Results Phys.* **2018**, *8*, 1268–1274. [CrossRef]
39. Yalcin, F.; Ilbeyli, N.; Demirbilek, M.; Yalcin, M.G.; Gunes, A.; Kaygusuz, A.; Ozmen, S.F. Estimation of natural radionuclides' concentration of the plutonic rocks in the Sakarya zone, Turkey using multivariate statistical methods. *Symmetry* **2020**, *12*, 1048. [CrossRef]
40. Hanfi, M.Y.; Abdel Gawad, A.E.; Eliwa, H.; Ali, K.; Taki, M.M.; Sayyed, M.I.; Khandaker, M.U.; Bradley, D.A. Assessment of radioactivity in Granitoids at Nikeiba, Southeastern Desert, Egypt; radionuclides concentrations and radiological hazard parameters. *Radiat. Phys. Chem.* **2022**, *2022*, 110113. [CrossRef]
41. Ravisankar, R.; Chandramohan, J.; Chandrasekaran, A.; Prakash, J.P.; Vijayalakshmi, I.; Vijayagopal, P.; Venkatraman, B. Assessments of radioactivity concentration of natural radionuclides and radiological hazard indices in sediment samples from the East coast of Tamilnadu, India with statistical approach. *Mar. Pollut. Bull.* **2015**, *97*, 419–430. [CrossRef]